Electron nuclear double resonance of interstitial iron in silicon

S. Greulich-Weber and J. R. Niklas
Fachbereich Physik Universität-GH Paderborn, Warburger Strasse 100 A, 4790 Paderborn, Federal Republic of Germany

E. R. Weber
Department of Materials Science and Mineral Engineering, University of California, Berkeley, California 94720

J. M. Spaeth
Fachbereich Physik Universität-GH Paderborn, Warburger Strasse 100 A, 4790 Paderborn Federal Republic of Germany
(Received 27 March 1984)

We report on the first electron nuclear double-resonance investigation of an interstitial deep-level defect in silicon. For interstitial iron the superhyperfine interactions with six shells of neighbor nuclei comprising 42 silicon atoms could be resolved and determined. The localization of the two paramagnetic $3d$ electrons ($3d^8$) at the Fe_i^0 atom could be estimated to be between 80% and 95%. The superhyperfine data are discussed with a simple model for the defect wave function. It is shown that exchange polarization plays a major role in determining the superhyperfine interactions.

I. INTRODUCTION

Electron nuclear double-resonance (ENDOR) investigations of substitutional impurities in silicon were performed more than 20 years ago on shallow donors.[1] These experiments yielded valuable information on the superhyperfine interactions of the unpaired donor electron with many surrounding shells of silicon atoms. The data were compared with the effective-mass theory of shallow donor states.[2] For the chalcogenides S and Te, believed to be on substitutional sites and which form so-called "deep impurities," ENDOR results were published as well.[3,4] A satisfactory theoretical explanation of the measured distribution of the unpaired spin density of those deep levels has not yet been achieved.[3,5] From the analysis of the ENDOR data it is not yet clear whether the chalcogenides are substitutional or interstitial. This question can only be settled if a satisfactory theory becomes available, since this cannot be concluded from the ENDOR experiments alone.[3,4]

For interstitial impurities in silicon, ENDOR investigations resolving the superhyperfine interactions with the surrounding silicon nuclei have not yet been reported. Transition elements of the $3d$ row prefer interstitial sites in thermal equilibrium at high temperatures.[6] After sufficiently rapid quenching the ESR spectra of interstitial Cr, Mn, and Fe can be measured as first described by Ludwig and Woodbury.[7] In this paper Fe in Si has been chosen for the first ENDOR investigation of an interstitial impurity in silicon. From the ESR experiments it follows that iron is quenched in as Fe_i^0 in a $S=1$ spin triplet state.[8–10] In a recent ESR study at high microwave power the superhyperfine (shf) structure of the ESR spectrum could partly be resolved[11] and the superhyperfine interactions with several neighbor shells were deduced. However, comparison with the present ENDOR study shows that in Si due to the low abundancy of the magnetic isotope ^{29}Si of only 4.7 at. % it is not straightforward to derive the shf interactions from the ESR spectrum. With ENDOR the shf interactions with 6 shells of neighbor nuclei, obtaining a total of 42 si atoms, could be determined with high precision. It was the aim of this investigation to determine the unpaired spin density around the interstitial Fe in order to provide an experimental basis for a highly localized, well-defined deep-level defect for theoretical calculations.

II. EXPERIMENTAL

Samples of dislocation-free floating-zone p silicon with 10^{13} B/cm^3 (Wacker Chemitronic) of dimensions typically $4\times4\times20$ mm^3 were mechanically and chemically polished and iron plated onto the four side faces in vacuum. The diffusion treatment was performed at 1250 °C for 30 min in a vertical SiC tube furnace and the sample was subsequently quenched in diffusion pump oil. Then a surface layer of more than 100 μm was mechanically and chemically removed. The samples were stored at 77 K until the ENDOR measurements. The concentration of interstitial Fe_i^0 thus achieved was 10^{16}/cm^3.[12]

The ENDOR measurements were performed in a computer controlled homodyne X-band spectrometer using a GaAs—field-effect transistor low-noise microwave preamplifier to improve the signal-to-noise ratio at the low-modulation frequencies necessary for ENDOR.[13] The ENDOR signals were obtained at $T=20$ K at a microwave power level of about 10^{-5} W by observing the microwave absorption signal. The rf transmitter was chopped at 800 Hz. The crystal orientation was varied in steps of 2°, rotating it by about 120° in a (110) plane.

III. EXPERIMENTAL RESULTS

A. ESR measurements

The electron-spin-resonance (ESR) spectra of interstitial iron in silicon consists of strain-broadened $\Delta m_s = \pm 1$ ESR transitions for a $S=1$ spin system ($3d^8$) at $g=2.070$. However, using high microwave power (20 mW), a double quantum transition between the $m_s=-1$ and $m_s=+1$ levels dominates the spectrum and is superimposed on the strain-broadened single-quantum transitions.[8] Figure 1(a) shows our measurements of the double-quantum X-band ESR spectrum for $\vec{B}_0 \| [111]$ at 25 K. A superhyperfine structure due to the interaction with ^{29}Si nuclei is partly resolved.

B. ENDOR measurements

Figure 2(a) shows an ENDOR spectrum as measured at 20 K. The most prominent feature is that the line at 2.7 MHz, which is the Larmor frequency of the free ^{29}Si nuclei, is about two orders of magnitude higher than the lines of ^{29}Si nuclei interacting with the unpaired electrons. Their signal-to-noise ratio was only about 5:1. Furthermore, a strong background signal was observed, much stronger than the lines of the interacting nuclei. In Fig. 2(b) this background was subtracted with a special algorithm. Now the signal-to-noise ratio of the spectrum is seen more clearly. This noise can be reduced drastically by digital filtering[14–16] as shown in Fig. 2(c). Finally, the resolution of superimposed peaks is improved by the application of a deconvolution algorithm[17] [Fig. 2(d)]. The peak positions of the ENDOR lines in Fig. 2(d) were automatically determined with a special peak-search algorithm.[17]

These computer-aided mathematical procedures were applied to all ENDOR spectra measured for different crystal orientations. Figures 3(a) and 3(b) show the angular dependence of the ENDOR lines thus determined experimentally for rotation of the crystal in a (110) plane. The dots are the experimental points, the size of which is a measure of the relative height of the lines. The spectra were analyzed with the usual spin Hamiltonian including the hyperfine interaction

$$H = g_e \mu_B \hat{S}_z + \sum_i (I_i \tilde{A}_i S - g_{ni} \mu_n \hat{B}_0 \hat{I}_i) , \qquad (1)$$

where the symbols have their usual meaning.[18] The sum runs over all ^{29}Si neighbor nuclei interacting with the unpaired electron spins. The curves drawn in Figs. 3(a) and 3(b) are the calculated ENDOR angular dependencies using the spin Hamiltonian (1) after fitting the tensor parameters for each neighbor nucleus i.

The number of ENDOR lines for each neighbor ^{29}Si nucleus ($I=\frac{1}{2}$) is the same for $S=\frac{1}{2}$ and $S=1$, namely, 2. Therefore, a confirmation of $S=1$ by ENDOR was attempted by choosing a particular neighbor shell, where the anisotropic interaction is large and prevails over the isotropic one.

When evaluating the spin Hamiltonian according to Eq. (1) with perturbation theory, in our case a second-order term enters, which contains m_s.[19] Figures 4(a) and 4(b) show the comparison of the calculated angular dependence of [111]-type neighbors with strong anisotropic interaction assuming $S=\frac{1}{2}$ and $S=1$. The fit for $S=1$, Fig. 4(b), is clearly better, confirming $S=1$ for the spin state of Fe_i^0 in Si.

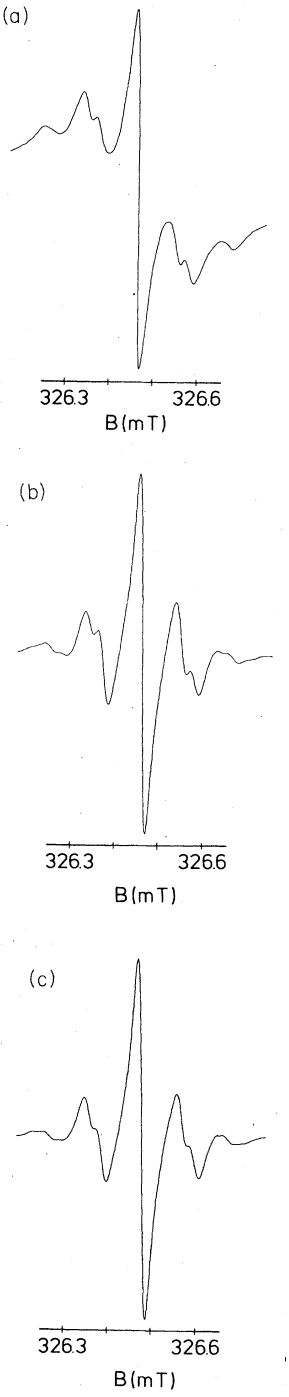

FIG. 1. (a) Double quantum ESR spectrum of Fe_i^0 at X-band, $T=25$ K for $B_0 \| [111]$. (b) Simulation of the ESR spectrum of Fig. 1(a) using all superhyperfine interactions determined by ENDOR. (c) Simulation of the ESR spectrum of Fig. 1(a) using the superhyperfine interactions determined by ENDOR omitting those of the second-shell (100) neighbors.

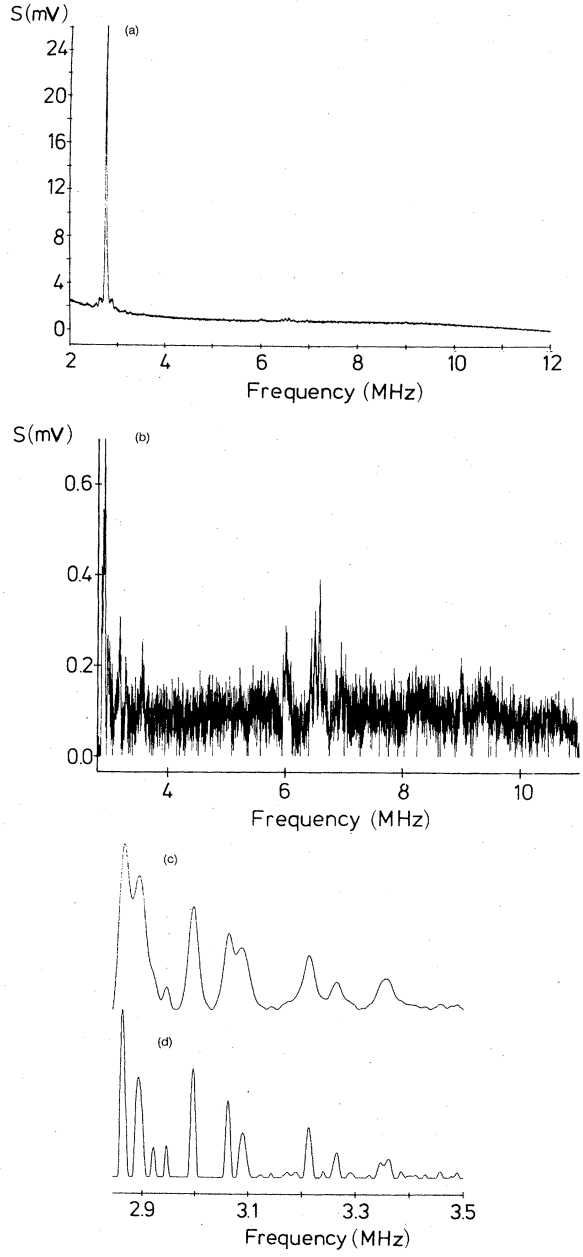

FIG. 2. (a) Measured ENDOR spectrum at $T=20$ K, $B_0=327.73$ mT, X-band, for B_0 approximately 20° off the [100] direction in a (110) plane. (b) Measured ENDOR spectrum of Fig. 2(a) after subtraction of the background. (c) Part of the spectrum of Fig. 3(b) after digital filtering. (d) Resolution enhancement of peaks in the spectrum of Fig. 2(c) by deconvolution.

In Table I the superhyperfine interaction parameters are given in terms of the isotropic shf constant a and the anisotropic shf constants b and b', where b' describes the deviation from axial symmetry. They are related to the principal values of $\tilde{A}$ by

$$A_{xx}=a-b+b',\quad A_{yy}=a-b-b',\quad A_{zz}=a+2b\ . \tag{2}$$

The orientations of the shf tensors are also given.

The analysis of the ENDOR angular dependence shows

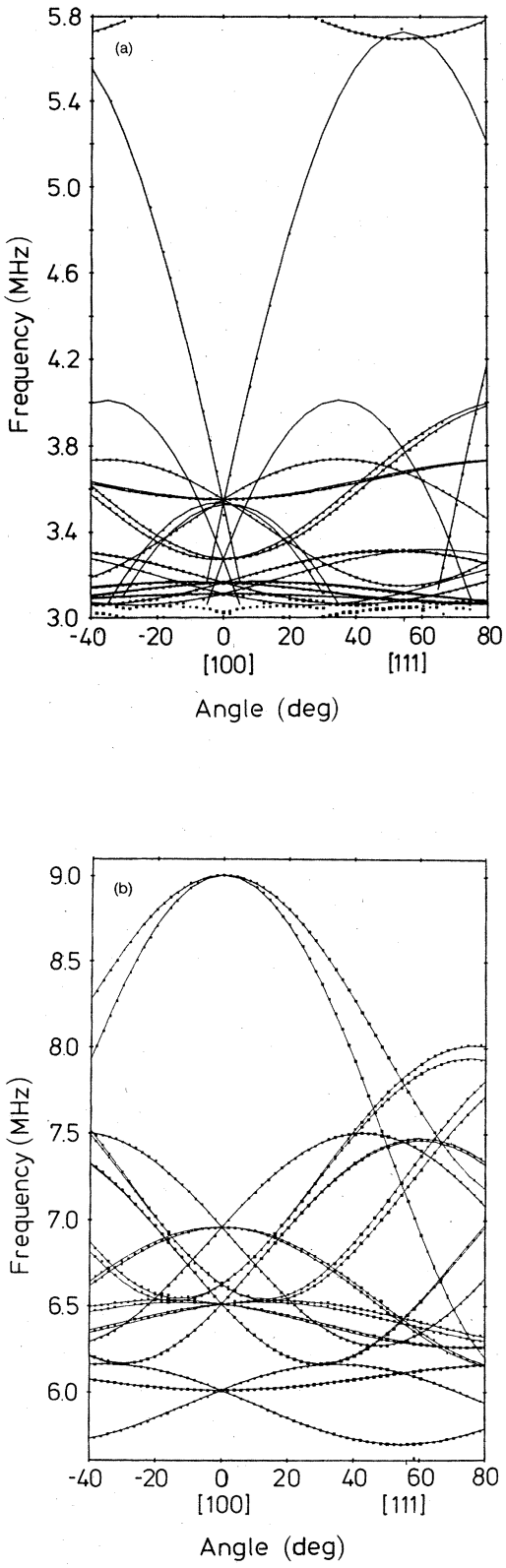

FIG. 3. Angular dependence of the ENDOR lines for rotating the crystal in a (110) plane. The dots are the experimental ENDOR line positions, the drawn curves are the calculated angular dependences calculated with the spin Hamiltonian parameters determined from the analysis of the spectra.

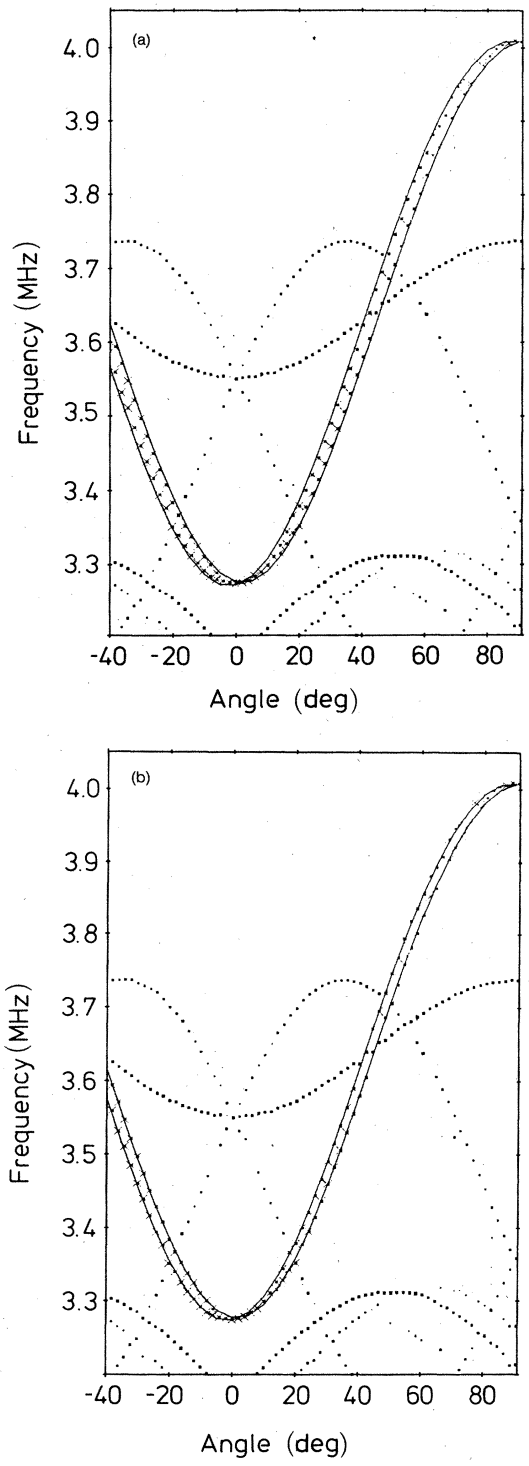

FIG. 4. (a) Angular dependence of the first-shell (111) neighbor nuclei and calculated angular dependence assuming $S=\frac{1}{2}$. (b) Angular dependence of the first-shell (111) neighbor nuclei and calculated angular dependence assuming $S=1$.

that Fe^0 must be either at the interstitial site with tetrahedral symmetry or substitutional. This cannot be distinguished from the analysis of the angular dependence, since in both cases neighbor nuclei with the same symmetry type surround the atom.[3,4] We found interactions with three different shells of neighbors with a [111] symmetry. Their shf tensor are axially symmetric and oriented along [111]. Each shell contains four nuclei. Furthermore, we found interactions with one shell of neighbors with [100] symmetry. There are six neighbors in this shell, the z axis of the interaction tensor is the [100] connection line to Fe^0, which is a twofold rotation axis (see Fig. 5). Finally, there are interactions with two shells with [110] symmetry, which each contains 12 nuclei. The shf axis with largest interaction lies in a (110) plane, which contains the Fe_i^0. Their angle with respect to a [111] direction is given in Table I (see also Fig. 5). No ENDOR lines due to low-symmetry neighbors were found.

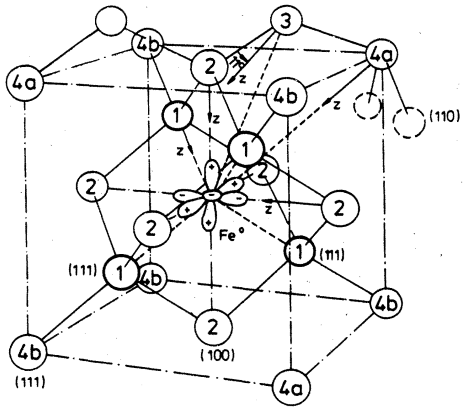

FIG. 5. Model of interstitial Fe^0 centers and five neighbor Si shells, the superhyperfine interaction of which was determined.

It should be noted that the relative sign of a and b is not always the same. From the angular dependence, however, only the relative signs of a and b can be determined. In Table I, b was chosen to be positive (see Sec. IV).

IV. DISCUSSION

Before an attempt to interpret the measured shf data was made [which turned out to be not a simple matter (see below)], we wanted to make sure that all measured shf interactions really belong to the same Fe_i^0 center. The possibility had to be excluded that we had, without knowing it, saturated another ESR spectrum lying under the Fe_i^0 spectrum and measured its ENDOR lines as well. Therefore, we simulated the double quantum ESR spectrum of Fig. 1(a), which shows a partially resolved shf structure taking all the shf interactions as determined from the ENDOR spectra into account. A computer program was developed for this. It calculated all possible magnetic configurations of neighbor nuclei due to the low ^{29}Si abundance of 4.7 at. %. Figure 1(b) shows the simulated ESR spectrum, which agrees very well indeed with the experimental one. Figure 1(c) shows the simulated spectrum, if the interactions with the six nuclei of (100) symmetry are taken out. A noticeable difference indicates that the simulation would show if this neighbor shell belonged to a different center. The same is true for the other shells, supporting the conclusion that all the measured shf data belong to Si nuclei surrounding the interstitial iron atom.

TABLE I. Parameters and orientation of shf tensors of ^{29}Si neighbors in Si:Fe_i^0 (in MHz). The experimental uncertainty is ±0.01 MHz.

Type	a	b	b'	Z_{shf}
[111]	0.16	1.40	0	[111]
[111]	−0.78	0.20	0	[111]
[111]	−3.25	0.16	0	[111]
[100]	4.64	0.80	0.52	[100]
[110]	3.87	0.44	−0.07	$\langle(Z_{shf},[111])=11°$
[110]	0.38	0.09	0.002	$\langle(Z_{shf},[111])=2.6°$

From the analysis of the ENDOR spectrum alone an assignment of the measured shf interactions to a particular shell of neighbors is not possible, only the symmetry type can be determined. Therefore, a theoretical estimate of the interactions must be made, if an assignment is attempted. First, the shf parameters can be analyzed with the traditional approach as described by Watkins and Corbett.[20] It assumes that an unpaired electron localized 100% within a silicon 3s orbital causes an isotropic hyperfine interaction of $a_f=4150$ MHz, and in a silicon 3p orbital an anisotropic interaction with $b_f=101$ MHz. Comparison of these values with the results compiled in Table I shows that the anisotropic shf interaction determines the fraction of the resonance electrons at the surrounding atoms. Localization values near 1% per atom can be calculated for the three shells with the strongest shf interactions. Identifying these shells with the three neighboring shells of Fe_i^0, which consist of 22 atoms, a delocalization near 20% of the resonance electron wave functions can thus be estimated.

However, this approach is misleading in the case of such a highly localized defect, since it neglects the dipole-dipole interaction of the two 3d electrons with the neighboring nuclei:[18]

$$b=\frac{1}{2}\frac{1}{8\pi}\mu_0 g_e\mu_B g_n\mu_n\int\frac{3\cos^2\theta-1}{\gamma^2}\,|\psi_{Fe_i^0}|^2 dV\,. \qquad (3)$$

Table II shows a comparison of the anisotropic interactions b^d calculated assuming point dipoles for the two Fe 3d electrons and the experimental b values, which are ordered according to decreasing b^d values (for shells 4a and b, see below). The good agreement between the experimental b and b^d allows an assignment of the experimental a and b values to the shells 1–5 (see Fig. 5, where the shells are indicated by numbers).

According to Ludwig and Woodbury[8] and more recent calculations of the energy levels of Fe_i^0 (Refs. 21–24) the unpaired electrons are in the two 3d orbitals with e_g symmetry; that is, in 3_{dz^2} and $3d_{x-y^2}$, respectively. Integrating in Eq. (3) over those orbitals yields within 1% the same b values as in the point-dipole approximation already for the nearest shells.[25]

Table II shows clearly that the largest part of the experimental b values can be accounted for by dipole-dipole interaction. The remaining differences could be explained by only 5% delocalization of the unpaired electrons. This value might be an underestimation as it is difficult to calculate reliably the dipole-dipole interaction with the directly adjacent silicon atoms. Yet this discussion shows that the paramagnetic 3d wave functions will be localized between 80% and 95% at the impurity atom, in accordance with the picture of Fe_i^0 as a highly localized defect.

Assuming a substitutional site for Fe_i^0 there is no agreement between b_{expt} and b^d, e.g., for the [100] neighbors the discrepancy is by a factor of 8. This simple estimate is in agreement with all other evidence that Fe^0 is interstitial.[8,12]

Table II shows that the third-shell [110] neighbors have the largest discrepancies between b_{exp} and b^d. Also the orientation Z_{shf} of their shf tensor (see Table I) is not along the connecting line to the Fe^0 atom, which would be the case for a predominantly point dipole-dipole interaction. It deviates by 18° from this line, as indicated in Fig. 5. It is nearer to the [111] direction, connecting the third shell with the neighboring second-shell Si atoms. This points to the fact that at shell 3 the superhyperfine interactions are due to a transfer effect via shell 2. It is, however, surprising that a is nearly as large as in shell 2, where the atoms are immediate neighbors to the Fe^0 3d orbitals and that a is very small for the shell-1 neighbors. It is not obvious why the transfer effect from shell-2 neighbors should be different to shell-3 and shell-1 neighbors. The value of b seems to be reasonably well explained in shells 4a and 4b. However, the negative a values of rather large magnitude point to the existence of

TABLE II. Comparison of the experimental shf data with the theoretical anisotropic shf constants assuming point dipole interactions (MHz).

Shell	Symmetry	a	b	b^d	Distance (Å)
1	[111]	0.16	1.40	1.25	2.352
2	[100]	4.64	0.80	0.82	2.715
3	[110]	3.87	0.44	0.18	4.503
4a	[111]	−3.25	0.16	0.16	4.703
4b	[111]	−0.78	0.20	0.16	4.703
5	[110]	0.38	0.09	0.08	5.918

an exchange polarization (see below).

The isotropic shf constant of a nucleus at the site r_n is given by

$$a(r_n)=\tfrac{1}{2}\tfrac{2}{3}\mu_0 g_0 \mu_B g_n \mu_n \rho(r_n) \tag{4}$$

where $\rho(r_n)$ is the unpaired spin density at the nuclear site r_n due to the two $3d$ electrons. The experimentally determined highly-localized nature of the defect suggests trying an interpretation of the hyperfine data using approximations which proved to be successful in ionic solids.

The direct contribution of the $3d$ electrons already at the shell-1 and shell-2 neighbors is only very small and cannot explain the measured values. An estimate of its magnitude can be attempted by assuming that the Si sp^3 hybrids occupy the regular Si lattice positions. Covalency between them is neglected. The wave function of the defect is then the Slater determinant.

$$\psi_{\mathrm{Fe}_i^0}=\frac{1}{\sqrt{n!}}\left|\psi^{\uparrow}_{dz^2}\psi^{\uparrow}_{d(x^2-y^2)}\psi^{\uparrow}_i\psi^{\downarrow}_i\cdots\psi^{\uparrow}_n\psi^{\downarrow}_n\right| , \tag{5}$$

where ψ_i denote the sp^3 Si wave functions. (The inner shells are neglected.) Provided all wave functions entering the Slater determinant are mutually orthogonal, the spin density at the site r_n is given by

$$\rho(r_n)=|\psi_{dz^2}(r_n)|^2+|\psi_{d(x^2-y^2)}(r_n)|^2 . \tag{6}$$

The two $3d$ functions ψ_{dz^2} and $\psi_{d(x^2-y^2)}$ are not orthogonal to the lattice functions. They must be orthogonalized to the lattice orbitals, which leads to admixtures of lattice orbitals into the $3d$ functions.[26] Considering first only shell-1 and shell-2 neighbors and using the Schmidt orthogonalization procedure,[26] this leads to admixtures of ψ_{3s} ($\mathrm{Si}^{(2)}$) and $\psi_{3p\sigma}$ ($\mathrm{Si}^{(2)}$) (along [100]; see Fig. 6) orbitals of shell-2 neighbors into ψ_{3dz^2}. The admixture coefficients are the overlap integrals between ψ_{dz^2} and ψ_{3s} ($\mathrm{Si}^{(2)}$), and

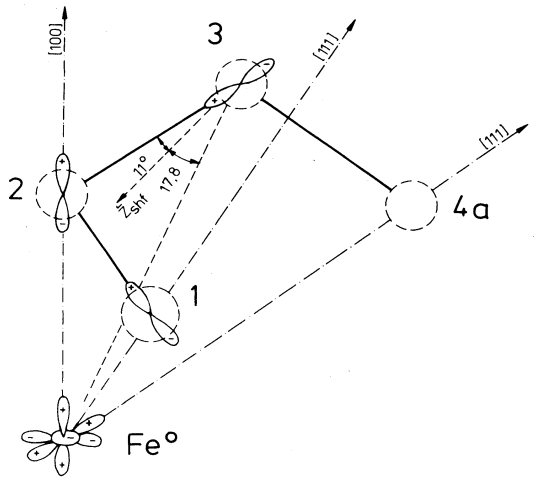

FIG. 6. Schematic representation of the orbitals contributing to the transferred superhyperfine interaction of shells 1 and 3 via shell 2.

$\psi_{3p\sigma}$ ($\mathrm{Si}^{(2)}$), respectively. Because of symmetry no orbitals of shell-1 and shell-2 neighbors are admixed into $\psi_{d(x^2-y^2)}$; all overlap integrals vanish. Using Eqs. (6) and (3) and the thus orthogonalized wave functions ψ_{dz^2} and $\psi_{d(x^2-y^2)}$, the theoretical values for a and b for shells 1 and 2 are obtained (Tables III and IV model 1). The agreement is surprisingly good regarding the crude theoretical model. If shell-2 neighbors were distorted outwards by $\sim 3\%$ the agreement would be almost perfect. However, the higher shells are not explained in this simple model.

Transferred hyperfine interactions were often observed in ionic crystals. Their order of magnitude could be explained by applying the Löwdin orthogonalization method.[19,27,28] The leading term determining a is given by the mutual overlap of the orbitals of neighboring atoms.[19,27] In our simple model (see Fig. 6),

$$a(r_n)\simeq\frac{a_f}{2}\left[\frac{1}{\sqrt{3}}\langle\psi_{dz^2}|\psi_{3p\sigma}(\mathrm{Si}^{(2)})\rangle\langle\psi_{3p\sigma}(\mathrm{Si}^{(2)})|\psi_{3s}(\mathrm{Si}^{(n)})\rangle+\langle\psi_{dz^2}|\psi_{3s}(\mathrm{Si}^{(2)})\rangle\langle\psi_{3s}(\mathrm{Si}^{(2)})|\psi_{3s}(\mathrm{Si}^{(n)})\rangle\right]^2 . \tag{7}$$

This expression holds for both shell-1 and shell-3 neighbors; that is, $\mathrm{Si}^{(1)}$ and $\mathrm{Si}^{(3)}$ admixtures. Unfortunately, because of the phase of the $\psi_{3p\sigma}(\mathrm{Si}^{(2)})$ orbital, the two terms in Eq. (7) nearly cancel each other for shell-3 neighbors and add for shell-1 neighbors.

Similar arguments hold for the calculations of b. (See Tables III and IV, model 2, where effects due to normalization constants are neglected in view of the crude model). The difference in the transfer effect in shells 1 and 3 originates in the phase of the admixtured $\psi_{3p\sigma}(\mathrm{Si}^{(2)})$ orbital.

TABLE III. Comparison of the experimental isotropic shf constants with several theoretical approximations (MHz).

Shell	a_{expt}	$a_{\mathrm{model\ 1}}$	$a_{\mathrm{model\ 2}}$	$a_{\mathrm{model\ 3}}$
1	0.16	0	1.7	0.005
2	4.64	5.4	5.4	5.4
3	3.87	0	0.005	1.7
4*a*	−3.25	0	∼0	∼0
4*b*	−0.78	0	∼0	∼0

TABLE IV. Comparison of the experimental anisotropic superhyperfine constants with several theoretical approximations (MHz).

Shell	b_{expt}	$b_{\text{model 1}}$	$b_{\text{model 2}}$	$b_{\text{model 3}}$
1	1.40	1.25	1.25	1.25
2	0.80	1.0	1.0	1.0
3	0.44	0.17	0.17	0.22
4*a*	0.16	0.16	0.16	0.16
4*b*	0.20	0.16	0.16	0.16

The observation is, however, in contrast to the calculation with the Löwdin orthogonalization, which only includes the Pauli principle.[26] Formally, this can be remedied by considering a slight covalency between the Fe $\psi_{3d_{z^2}}$ orbital and the $\psi_{3p\sigma}(\mathrm{Si}^{(2)})$ orbital according to

$$\psi^{\lambda}_{dz^2}=N[\psi_{dz^2}-\lambda\psi_{3p}(\mathrm{Si}^{(2)})]\ ,\qquad N=(1+\lambda^2)^{-1/2}\ . \tag{8}$$

Neglecting the small deviation of N from 1, one then obtains for $a(r_n)$

$$a^{\lambda}(r_n)\simeq\frac{a_f}{2}\left[\lambda+\frac{1}{\sqrt{3}}\langle\psi_{dz^2}\,|\,\psi_{3p\sigma}(\mathrm{Si}^{(2)})\rangle\langle\psi_{3p\sigma}(\mathrm{Si}^{(2)})\,|\,\Psi_{3s}(\mathrm{Si}^{(n)})\rangle+\langle\psi_{dz^2}\,|\,\psi_{3s}(\mathrm{Si}^{(2)})\rangle\langle\psi_{3s}(\mathrm{Si}^{(2)})\,|\,\psi_{3s}(\mathrm{Si}^{(n)})\rangle\right]^2 . \tag{9}$$

Choosing $\lambda=2\,|\,\langle\psi_{dz^2}\,|\,\psi_{3p\sigma}(\mathrm{Si}^{(2)})\rangle\,|=0.126$ just reversed the interference effect for shells 1 and 3, and the observed magnitude of the isotropic shf constants can then be approximately explained (see Table III, model 3). The anisotropic interaction of shell-3 neighbors is also improved, the z axis now is 19° off the [111] direction (see Fig. 6); that is, it is turned by about 10° from the connection line to the Fe^0 towards [111]. b is, however, too small (Table IV, model 3). In order to explain the experimental orientation and b value one would need four times as much admixture contributions along [111]; that is, 0.2 MHz along the connection line of $\mathrm{Si}^{(2)}-\mathrm{Si}^{(3)}$.

Why a covalent admixture is connected with a phase correlation is an open question. It apparently is needed to get different transfer effects for shells 1 and 3 as observed.

One further important point must be discussed, which is connected with the observation of negative spin density at shells 4*a* and *b*. Negative spin densities at Al nuclei were observed for several Al^{3+}-0^- centers in ionic crystals, where the Al^{3+} ions were situated in a nodal plane of the unpaired p orbital at the oxygen.[29–31] All overlap contributions vanish since the overlap integrals with s functions are zero. The negative spin density in such a situation is explained as being due to exchange polarization.[32–34] This effect is probably also observed directly for shells 4*a* and 4*b* nuclei. The p admixture of shell-3 neighbors along [111] connecting it to shell 2 has a large component "perpendicular" to shell-4*a* neighbors in the sense that they are in the nodal plane of the unpaired p orbitals (see Fig. 6). The exchange-polarization effect is expected to be larger for shell-4*a* neighbors compared to shell-4*b* neighbors, since they are nearer to the shell-3 neighbors in agreement with our results. This consideration led to the assignment of shells 4*a* and 4*b* to the measured shf interactions.

Clearly, the exchange polarization will also be operating between the p admixture of shell 2 and the core of shells 3 and 1, both with the same magnitude, since their perpendicular $\psi_{3p\sigma}(\mathrm{Si}^{(3)})$ components are the same, giving a negative contribution to a for both neighbors. On the other hand, the covalency between the Si neighbors neglected thus far will enhance the transfer effects. From the experimental results it seems that for the shell-1 and shell-3 neighbors these covalency effects must be compensated by the exchange polarization. It is probably because of this that our crude model discussed above yields approximately the experimental shf data. Possibly, exchange polarization effects between the two Fe3*d* orbitals and shell-1 neighbors are also contributing to explain their small value of a.

It was the aim of our estimate to point out that this highly localized interstitial model defect shows an interesting quantum-mechanical interference effect in spin-density transfer and that exchange polarization seems to play a very important role which, to our knowledge, has not yet been realized in discussing hyperfine properties of defects in silicon.

In conclusion, we have shown that the interstitial Fe^0 atom, although highly localized, comprises a complex of at least 42 Si neighbors when considering the effects of spin transfer. It seems a clear model system for a deep level and it is hoped that it will be possible to quantitatively explain its electronic structure in the future.

ACKNOWLEDGMENTS

The authors are indebted to H. Overhof, A. Zunger, and H. Katayáma-Yoshida for stimulating discussions.

[1]G. Feher, Phys. Rev. **114**, 1219 (1959).
[2]W. Kohn and J. M. Luttinger, Solid State Phys. **5**, 257 (1957).
[3]G. W. Ludwig, Phys. Rev. **137**, A1520 (1965).
[4]J. P. Niklas and J.-M. Spaeth, Solid State Commun. **46**, 121 (1983).
[5]S. Y. Ren, W. M. Hu, O. F. Sankey, and J. D. Dow, Phys. Rev. B **26**, 951 (1982).
[6]E. R. Weber, Appl. Phys. A **30**, 1 (1983).
[7]G. W. Ludwig and H. H. Woodbury, Solid State Phys. **13**, 223 (1962).
[8]G. W. Ludwig and H. H. Woodbury, Phys. Rev. **117**, 102 (1960).
[9]M. Berke, E. Weber, H. Alexander, H. Luft, and B. Elschner, Solid State Commun. **20**, 881 (1976).
[10]W. Gehlhoff and K. H. Segsa, Phys. Status Solidi A **41**, K21 (1977).
[11]E. G. Sieverts, S. H. Muller, C. A. J. Ammerlaan, and E. R. Weber, Solid State Commun. **47**, 631 (1983).
[12]E. R. Weber and H. G. Riotte, J. Appl. Phys. **51**, 1484 (1980).
[13]Ch. Hoentzsch, J. R. Niklas, and J.-M. Spaeth, Rev. Sci. Instrum. **49**, 1100 (1978).
[14]M. U. A. Bromba and H. Zielger, Anal. Chem. **51**, 1760 (1979).
[15]H. Ziegler, Appl. Spectrosc. **35**, 88 (1981).
[16]M. U. A. Bromba and H. Ziegler, Anal. Chem. **53**, 1583 (1981).
[17]J. R. Niklas (unpublished).
[18]A. Abragam and B. Bleaney, *Electron Paramagnetic Resonance of Transition Ions* (Clarendon, Oxford, 1970), p. 142.
[19]J. M. Spaeth, Z. Phys. **192**, 107 (1966).
[20]G. D. Watkins and J. W. Corbett, Phys. Rev. **134**, A1359 (1964).
[21]G. G. DeLeo, G. D. Watkins, and W. B. Fowler, Phys. Rev. B **23**, 1851 (1981).
[22]G. D. DeLeo, G. D. Watkins, and W. B. Fowler, Phys. Rev. B **25**, 4962 (1982).
[23]G. G. DeLeo, G. D. Watkins, and W. B. Fowler, Phys. Rev. B **25**, 4972 (1982).
[24]A. Zunger and U. Lindefelt, Phys. Rev. B **26**, 5989 (1982).
[25]A. N. Jette (private communication).
[26]B. S. Gourary and F. J. Adrian, Solid State Phys. **10**, 127 (1960).
[27]J. M. Spaeth and H. Seidel, Phys. Status Solidi B **46**, 323 (1971).
[28]A. M. Stoneham, *Theory of Defects in Solids* (Clarendon, Oxford, 1975).
[29]O. F. Schirmer, K. W. Blazey, and W. Berlinger, Phys. Rev. B **11**, 4201 (1975).
[30]M. Stapelbroek, R. H. Bartram, O. R. Gilliam, and D. P. Madacsi, Phys. Rev. B **13**, 1960 (1976).
[31]R. C. Barklie, J. R. Niklas, J. M. Spaeth, and R. H. Bartram, J. Phys. C **16**, 579 (1983).
[32]D. Ikenberry, A. N. Jette, and T. P. Das, Phys. Rev. B **1**, 2785 (1970).
[33]O. F. Schirmer, J. Phys. C **6**, 300 (1973).
[34]F. J. Adrian, A. N. Jette, and J. M. Spaeth (unpublished).